Electronic Supplementary Information (ESI)

Nucleation Mediated Interfacial Precipitation for Architectural Perovskite Films with Enhanced Photovoltaic Performance

Yu Yu[a,b], *Songwang Yang*[*,a], *Lei Lei*[a], *and Yan Liu*[*,a]

[a]CAS Key Laboratory of Materials for Energy Conversion, Shanghai Institute of Ceramics, Chinese Academy of Sciences, 588 Heshuo Road, Shanghai 201899, P. R. China.

[b]University of Chinese Academy of Sciences, Beijing 100039, P. R. China.

Kinetics curves drawn by classical nucleation theory calculation.

Homogeneous nucleation[1]. In classical nucleation theory, supersaturated solution in which the concentration of solute (c) exceeding the equilibrium solubility (c^*) possesses a high Gibbs free energy, when the supersaturation ($\Delta c = c - c^*$) achieves a critical point[1-4], nucleation will take place to reduce the energy and keep the system to be stable. The reduction of Gibbs free energy ΔG is the driving force for nucleation, ΔG consisted of two parts: ΔG_V and ΔG_S, which related to the change of volume energy and the change of surface energy respectively.

The chemical potential of per mole solute in supersaturated solution and saturated solution is μ, μ^*,

$$\mu = \mu^o + RT\ln\left(\frac{\zeta_1 c}{c^o}\right)$$

$$\mu^* = \mu^o + RT\ln\left(\frac{\zeta_2 c^*}{c^o}\right)$$

ζ_1 and ζ_2 is the activity coefficient, ζ_1 and ζ_2 can be regarded as the same when the change in concentration is not so much. The change of Gibbs free energy per unit volume of the new formed nucleus, $\Delta G_{V,0}$, is dependent on the c :

$$\Delta\mu = \mu^* - \mu = -RT\ln\frac{c}{c^*}$$

$$\Delta G_{V,0} = \frac{\Delta\mu}{V_m} = -\frac{k_B T}{\Omega}\ln\frac{c}{c^*} = -\frac{k_B T}{\Omega}\ln(1+\sigma)$$

Ω is the atomic volume, and V_m is the molar volume of new phase, relative supersaturation $\sigma = \frac{c - c^*}{c^*} = \frac{\Delta c}{c^*}$. Assuming a spherical nucleus is formed, the radius is *r*, the change of volume energy ΔG_V can be described by:

$$\Delta G_V = \frac{4}{3}\pi r^3 \Delta G_{V,0}$$

The formation of nucleus results in an increase in the surface energy, ΔG_S of the system:

$$\Delta G_S = 4\pi r^2 \gamma$$

γ is the surface energy per unit area, where ΔG_S is positive and ΔG_V is negative, the total change of Gibbs free energy for the formation of the nucleus, ΔG, is given by:

$$\Delta G = \Delta G_V + \Delta G_S = \frac{4}{3}\pi r^3 \Delta G_{V,0} + 4\pi r^2 \gamma$$

Only when $r > r^*$ the formed nucleus can grow up, the critical r^* can be obtained by $\frac{d \Delta G}{dr} = 0$:

$$r^* = -\frac{2r}{\Delta G_{V,0}}$$

Then the critical energy for homogeneous nucleation, ΔG_{Homo}^*, is defined by:

$$\Delta G_{Homo}^* = \frac{16\pi\gamma}{3 \Delta G_{V,0}^2}$$

Considering the $\Delta G_{V,0}$ have been defined as $\Delta G_{V,0} = -\frac{k_B T}{\Omega}\ln(1+\sigma)$, $\ln(1+\sigma) \sim \sigma$ can be

adopted when $\sigma + 1$ is very small, then the $\Delta G_{V,0}$ and ΔG^{*}_{Homo} are described by:

$$\Delta G_{V,0} = -\frac{k_B T}{\Omega}\sigma$$

$$\Delta G^{*}_{Homo} = \frac{16\pi\gamma\Omega^2}{3k_B^2 T^2 \sigma^2}$$

The steady state nucleation rate is an exponential function of the energy barrier in classical nucleation theory, here the rate of nucleation can be described by:

$$B_{Homo} = B_1^0 exp\left(-\frac{\Delta G^{*}_{Homo}}{k_B T}\right) = B_1^0 exp\left(-\frac{16\pi\gamma\Omega^2}{3k_B^3 T^3 \sigma^2}\right) = B_1^0 exp\left(-\frac{A}{\Delta c^2}\right)$$

$$A = \frac{16\pi\gamma c^{*2}\Omega^2}{3k_B^3 T^3}$$

The prefactor B_1^0 is the product of (I) the number density of molecules, is essentially the number of possible nucleation sites per unit volume, as for homogeneous nucleation the nucleus can form around any one of the molecules present (II) the rate at which molecules attach to the critical cluster causing it to grow and (III) Zeldovich factor, the probability of a critical cluster to cross the energy barrier.

Heterogeneous nucleation[1]. When nuclei form at preferential sites, the energy barrier to nucleation, ΔG^{*}_{Het} can be substantially reduced due to the newly created interfaces (nucleus/solution and nucleus/substrate) and the destroyed interface (solution/substrate). The extra interfacial energy terms can be incorporated into a shape factor,(θ), is defined by:

$$\Delta G_{Het}^{*} = \Delta G_{Homo}^{*} f(\theta)$$

$$f(\theta) = \frac{(2+\cos\theta)(1-\cos\theta)^2}{4}$$

The angle θ is the angle between the nucleus/substrate interface and the nucleus surface, called the contact angle, which always located in the range $0° \leq \theta \leq 90°$. Hence the nucleation rate differs from the case for homogeneous nucleation:

$$B_{Het} = B_2^0 exp\left(-\frac{\Delta G_{Het}^{*}}{k_B T}\right) = B_2^0 exp\left(-\frac{16\pi\gamma\Omega^2 f(\theta)}{3k_B^3 T^3 \sigma^2}\right) = B_2^0 exp\left(-\frac{Af(\theta)}{\Delta c^2}\right)$$

Secondary nucleation[3-5]. Empirical exponential formula is always adopted to describe secondary nucleation rate:

$$B_{Sec} = k_N G^i M_T^j$$

$$0.5 \leq i \leq 3$$

$$0.4 \leq j \leq 2$$

Where k_N is the nucleation kinetics constant, M_T is the suspension density of crystal slurry, i and j are empirical kinetic parameters. G is the crystal growth rate defined by change in length, G_M is the growth rate defined by change in mass and it is given by:

$$G_M = k_G \Delta c^l$$

k_G is the total coefficient of crystal growth, l is in the range of 1.54 ~ 1.6, the relationship between

G_M and G is given by:

$$G_M = \frac{3k_V}{k_a}\rho G$$

k_V and k_a are the volume shape factor and area shape factor, ρ is density of crystal, hence the secondary nucleation rate can be defined by:

$$B_{Sec} = k_N\left(\frac{k_a k_G}{3k_V\rho}\right)^i M_T^j \Delta c^{il} = E \Delta c^{il} = E \Delta c^{0.77\sim4.8}$$

$$E = k_N\left(\frac{k_a k_G}{3k_V\rho}\right)^i M_T^j$$

Crystal growth[3, 5]. The crystal growth rate is given in Secondary nucleation part above,

$$G = \frac{k_a k_G}{3k_V\rho}\Delta c^l = F \Delta c^{1.54\sim1.6}$$

$$F = \frac{k_a k_G}{3k_V\rho}$$

here G is the crystal growth rate defined by change in length, k_V and k_a are the volume shape factor and area shape factor, ρ is density of crystal.

References

1 R. P. Sear, *J. Phys.: Condens. Matter*, 2007, **19**, 033101.

2 C. Y. Tai and C.-Y. Shih, *J. Cryst. Growth*, 1996, **160**, 186-189.

3 G. D. Botsaris, *Secondary nucleation-a review*, Plenum Press, 1st edn, 1976, pp. 3-22.

4 J. Estrin and G. R. Youngquist, *Secondary nucleation and crystal growth as coupled phenomena*, Plenum Press, 1st edn, 1976, pp. 61-66.

5 C. Y. Sung, J. Estrin and G. R. Youngquist, *AIChE J.*, 1973, **19**, 957-962.

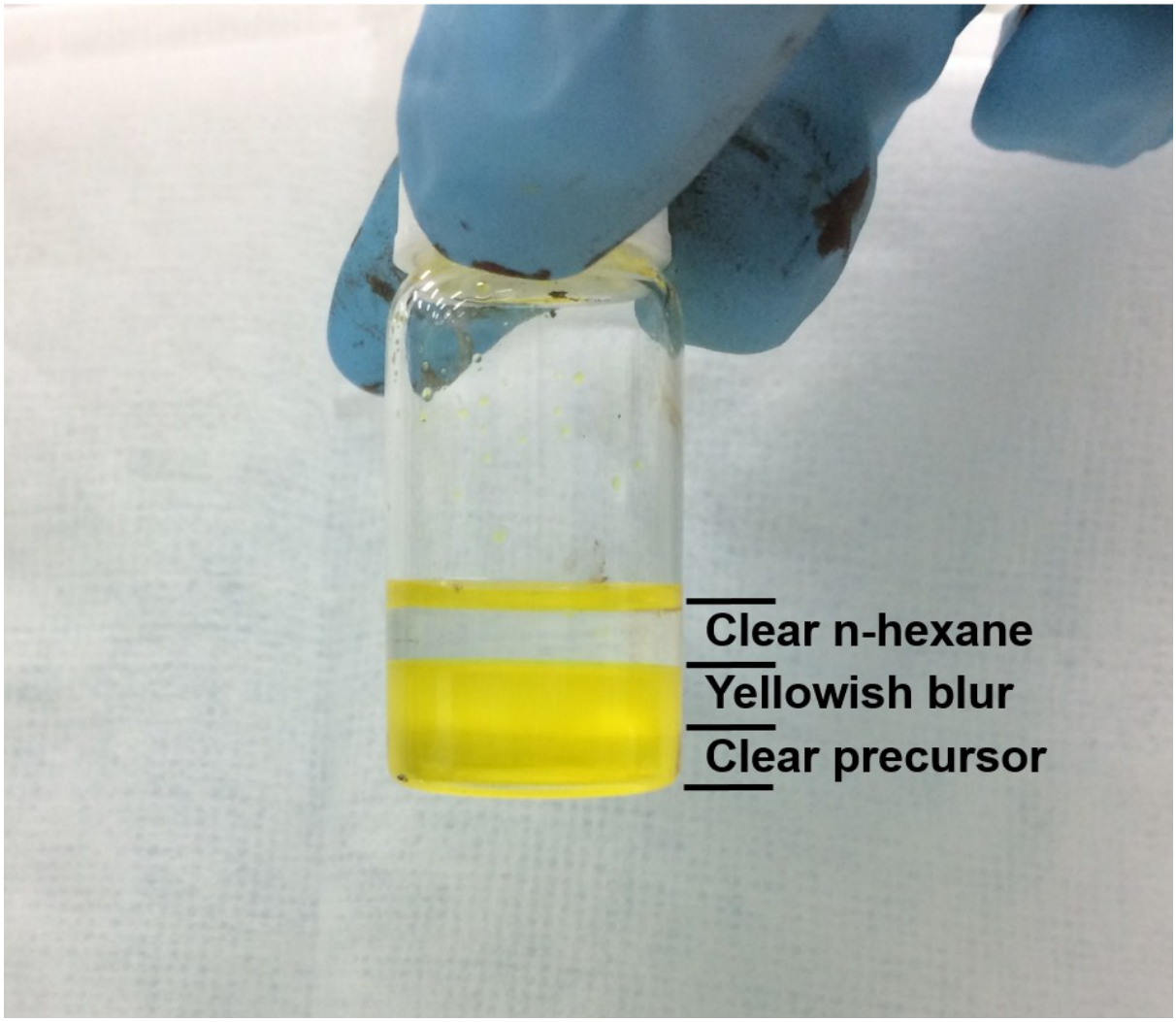

Figure S1. The picture of n-hexane/precursor interface. There are three layers. The top layer is the

clear n-hexane, the yellowish blur is presumable to be the intermediate nuclei in the middle, and the bottom is the clear yellow precursor solution.

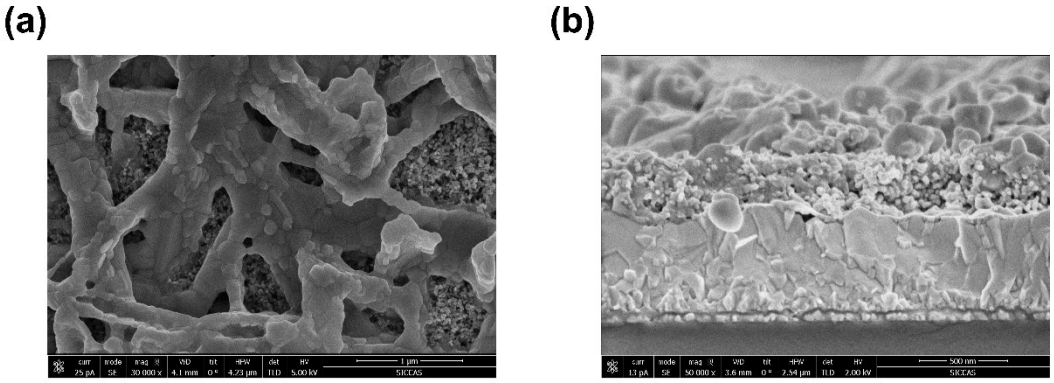

Figure S2. Top-view (a) and section-view (b) SEM images for perovskite films obtained by spin-coating precursor solution without adding DMSO (MAI and PbI_2 dissolved in DMF at a 1 : 1 molar ratio).

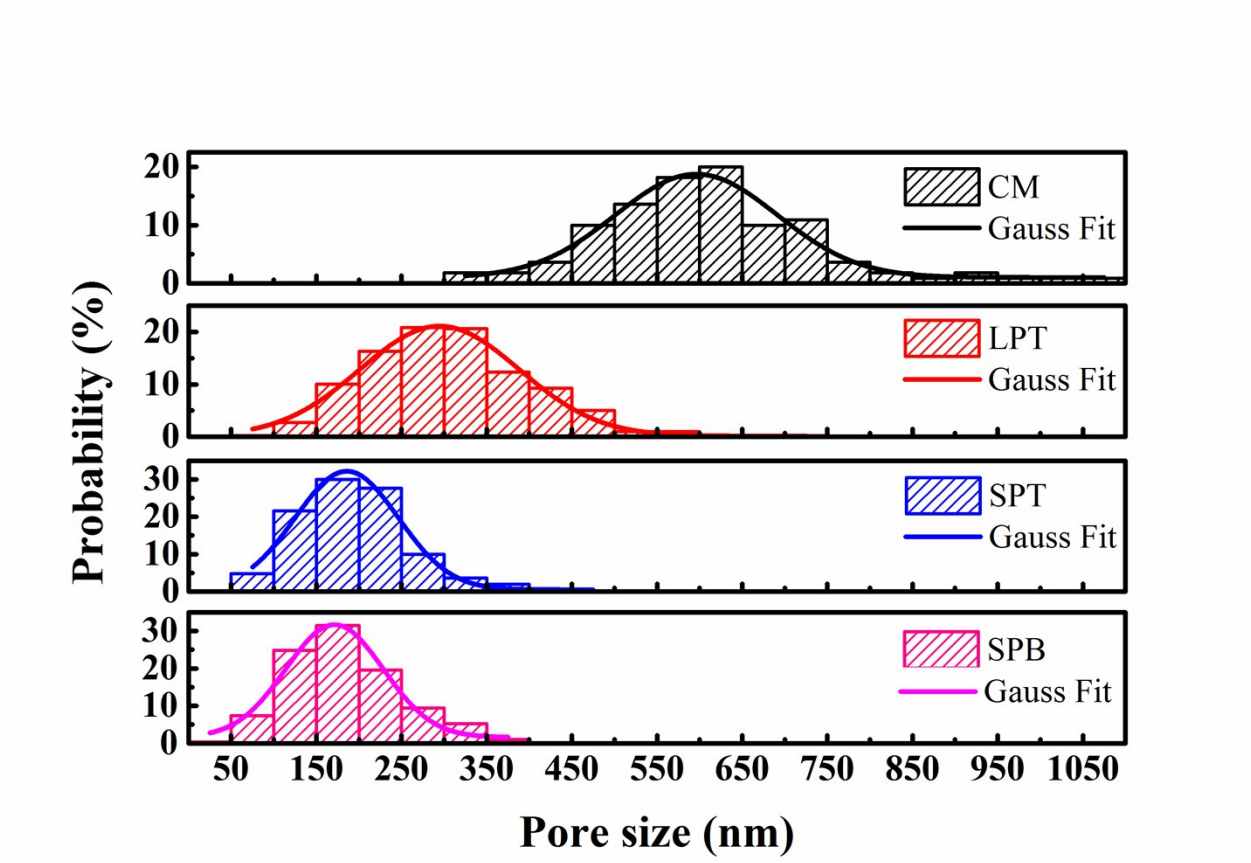

Figure S3. Pore size distribution of perovskite films prepared by different n-hexane dripping IP processes. The results were based on a statistical measurement of 110, 398, 251, 284 pores for CM, LPT, SPT and SPB films, respectively.

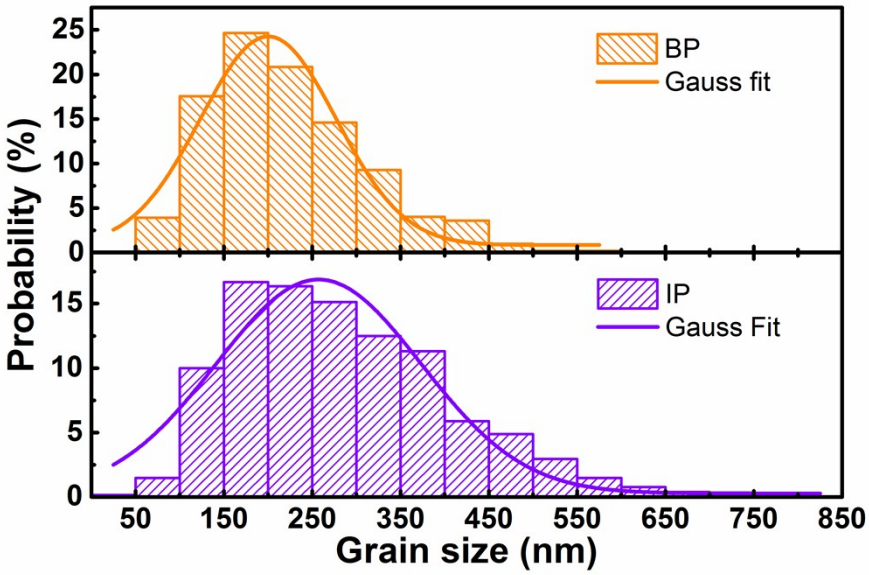

Figure S4. Grain size distributions of dense perovskite films made by BP and IP process. The distributions are based on a statistical measurement of 916 and 1290 grains for BP and IP process, respectively.

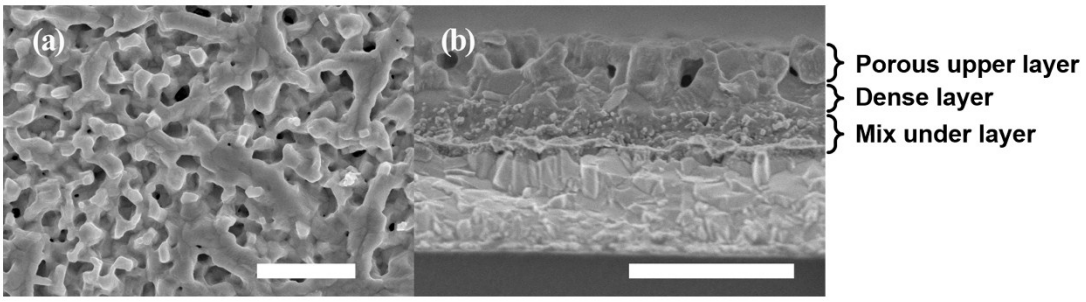

Figure S5. Top-view (a) and cross-section (b) SEM images of the film produced by petroleum ether induced IP method. 500 μl petroleum ether was dropped in one shot at the 6th s and lasting for 2s during spin-coating at 5000 rpm for 20 s. The scale bars correspond to 1 μm in length.

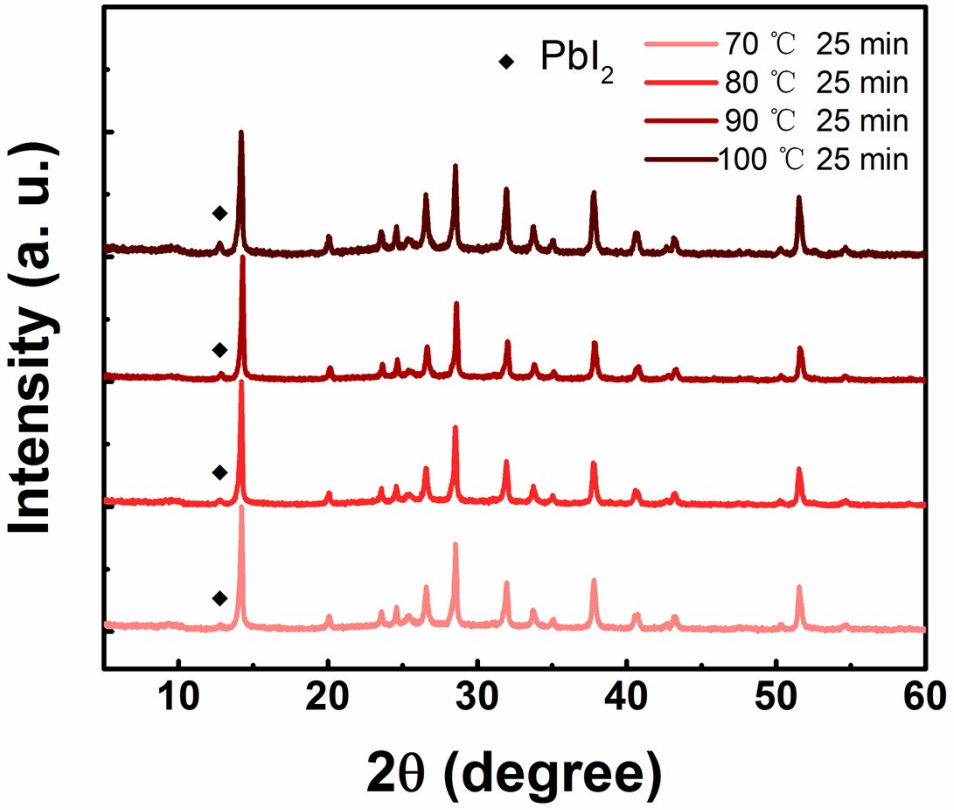

Figure S6. XRD patterns of films produced by n-hexane dripping method (IP) with different annealing conditions. The dripping procedure here is one-shot dripping 500 μl at the 6th s and lasting for 2s during spin-coating at 5000 rpm for 20s.

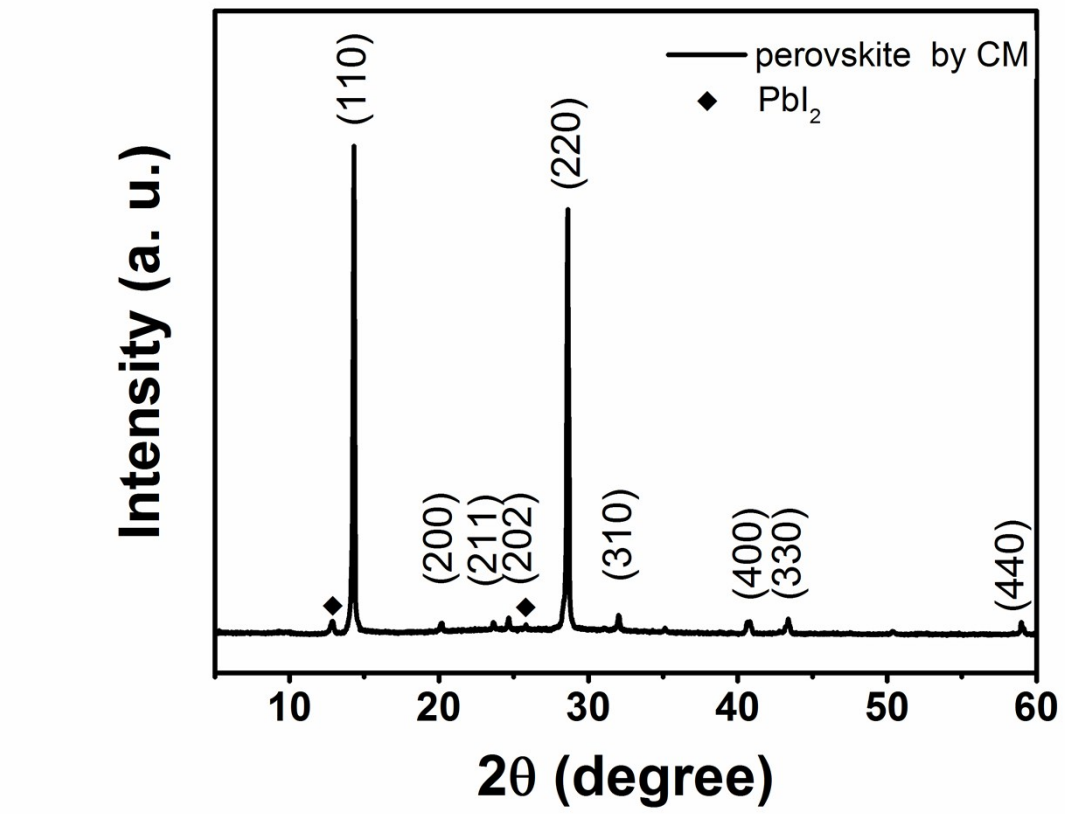

Figure S7. XRD pattern of the perovskite film deposited on the glass substrate by conventional one-step method (CM).

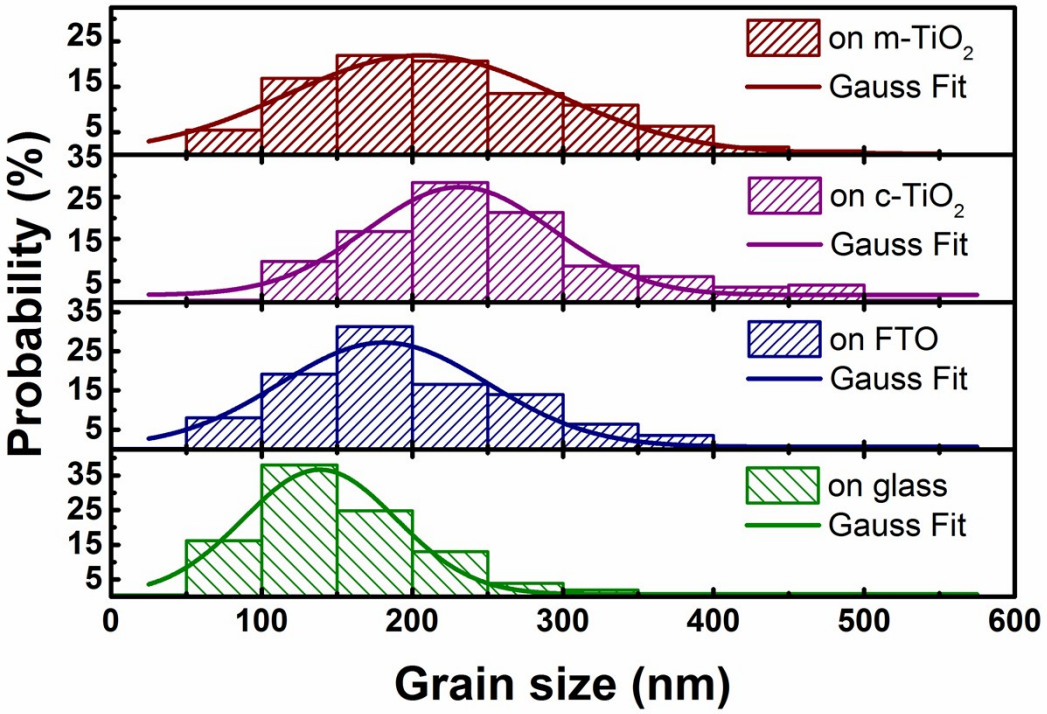

Figure S8. Grain size distributions of films prepared by bulk precipitation-based one-step solution method (BP) coated on m-TiO_2, c-TiO_2, FTO and glass substrates. The results were based on a statistical measurement of 235, 197, 421, 559 grains for the substrates of m-TiO_2, c-TiO_2, FTO and glass, respectively.

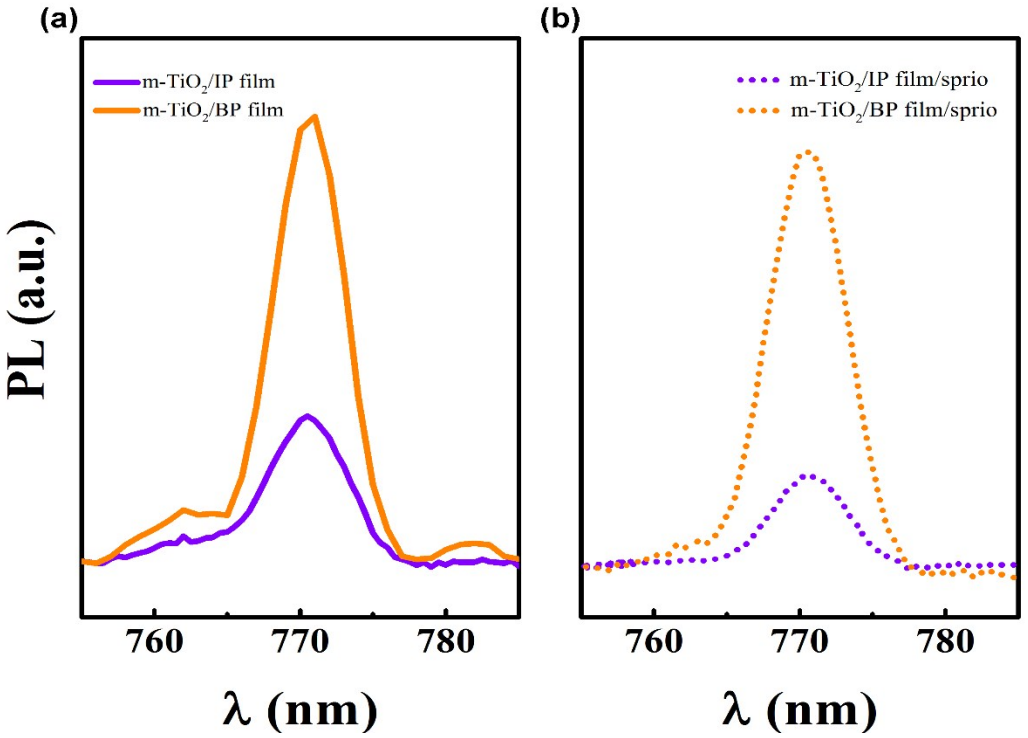

Figure S9. Carrier transfer between m-TiO_2/perovskite and perovskite/sprio interfaces. (a) PL spectra for a m-TiO_2/IP film sample and a m-TiO_2/BP film sample. (b) PL spectra for a m-TiO_2/IP film/sprio sample and a m-TiO_2/BP film/sprio sample. The peak between 765-775nm in (a) indicates the radiative recombination of free carriers, the diminished PL intensity in (b) indicates the efficient injection of free carriers into sprio. IP-SPT was used here for PL measurement.

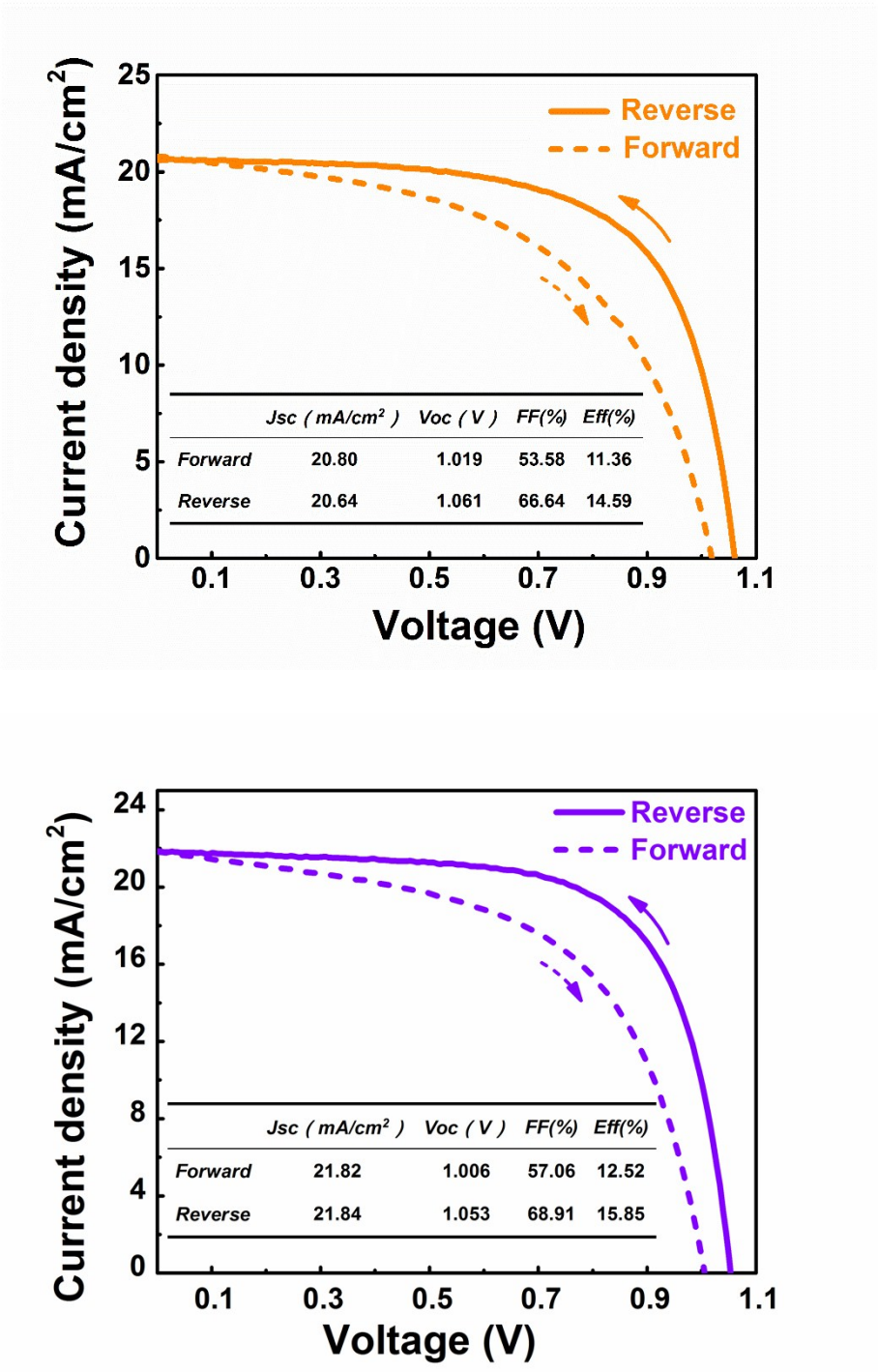

Figure S10. Hysteresis level. J-V curves for the solar cells based on the conventional dense perovskite film made by BP method (orange) and porous tri-layer perovskite film fabricated by IP method (IP-SPT, violet) measured by forward and reverse scans.

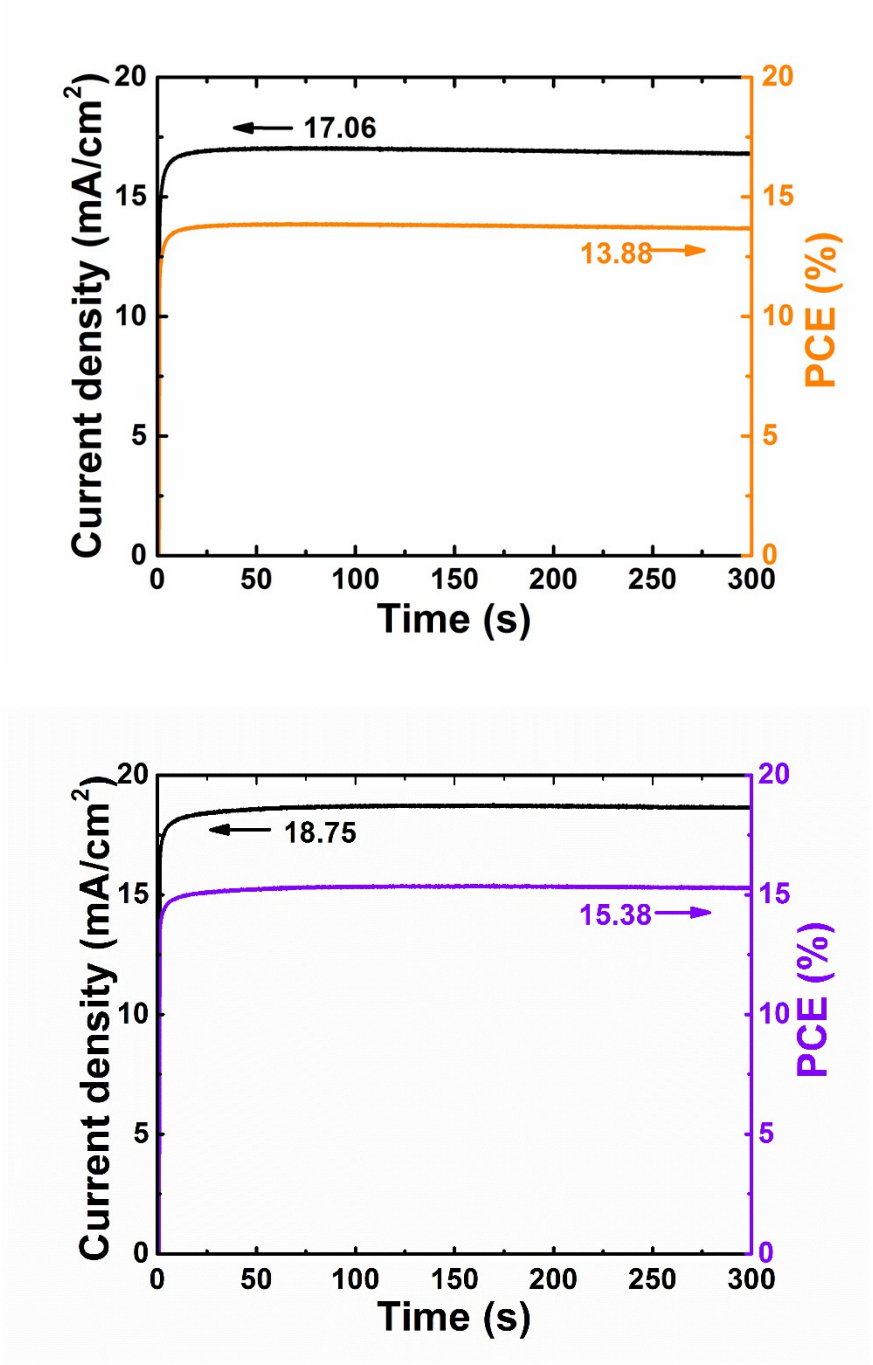

Figure S11. Steady-state output. Steady-state current along with the stabilized power output of perovskite solar cells fabricated by BP (orange) and IP (violet) method. Maximum power points were obtained according to J-V curves: 0.814 and 0.820 V for BP and IP respectively. IP-SPT sample was used for IP.

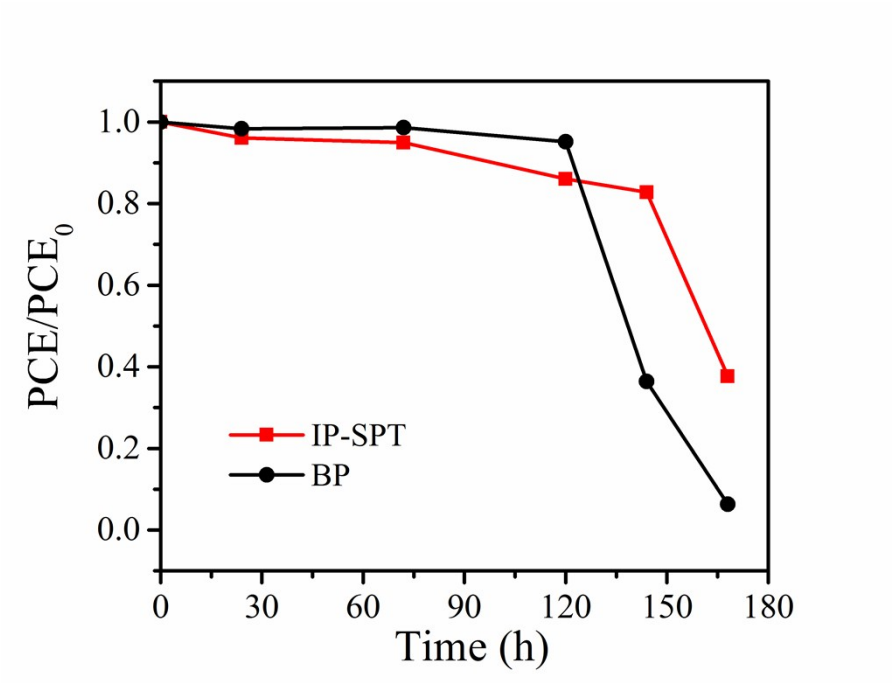

Figure S12. Normalized PCE versus time for BP and IP-SPT based devices. After approximately 120 hours both types of devices begin to rapidly decay in efficiency.

Table S1. Parameters of devices based on perovskite films prepared by CM, BP and different IP processes (LPT, SPT, SPB). Five cells were fabricated for each type of devices.

Device	***Jsc (mA/cm^2)***	***Voc (V)***	***FF (%)***	***Eff (%)***
CM-1	11.24	0.418	56.35	2.65
2	10.76	0.375	52.42	2.11
3	12.06	0.301	53.88	1.95
4	10.96	0.360	56.77	2.24
5	9.51	0.313	49.78	1.48
Average	10.91 ± 0.83	0.35 ± 0.04	53.84 ± 2.58	2.09 ± 0.38
BP-1	20.70	1.064	63.30	13.95
2	20.68	1.067	64.89	14.32
3	20.95	1.064	64.28	14.33
4	20.70	1.067	66.62	14.71
5	21.19	1.071	62.76	14.24
Average	20.84 ± 0.20	1.07 ± 0.01	64.37 ± 1.35	14.31 ± 0.24
IP-LPT-1	22.36	0.988	62.95	13.91
2	22.27	0.903	57.77	11.61
3	22.06	0.892	57.30	11.28
4	21.69	0.897	53.07	10.33
5	21.94	0.928	58.76	11.97
Average	22.06 ± 0.24	0.92 ± 0.04	57.97 ± 3.16	11.82 ± 1.18
IP-SPT-1	21.63	1.039	67.74	15.22
2	21.84	1.055	68.66	15.82
3	21.49	1.057	67.87	15.41
4	21.25	1.042	69.30	15.34
5	21.40	1.053	69.59	15.69
Average	21.52 ± 0.20	1.05 ± 0.01	68.63 ± 0.74	15.49 ± 0.22
IP-SPB-1	21.45	1.068	64.14	14.70
2	21.17	1.054	67.96	15.16
3	21.34	1.062	67.61	15.32
4	21.42	1.065	68.74	15.67
5	21.19	1.052	67.87	15.13
Average	21.31 ± 0.11	1.06 ± 0.01	67.30 ± 1.60	15.20 ± 0.32